Environ. Sci. Technol. **2003**, *37,* 908−914

Lead Sorption onto Ferrihydrite. 1. A Macroscopic and Spectroscopic Assessment

PARAS TRIVEDI,*,† JAMES A. DYER,†,‡ AND DONALD L. SPARKS†

Department of Plant and Soil Sciences, University of Delaware, Newark, Delaware 19717, and DuPont Engineering Technology, Brandywine Building, Wilmington, Delaware 19898

In this research, traditional macroscopic studies were complemented with XAS analyses to elucidate the mechanisms controlling Pb(II) sorption onto ferrihydrite as a function of pH, ionic strength, and adsorbate concentrations. Analyses of XANES and XAFS studies demonstrate that Pb(II) ions predominantly sorb onto ferrihydrite via inner-sphere complexation, not retaining their primary hydration shell upon sorption. At higher pH values (pH ≥5.0), edge-sharing bidentate complexes are mainly formed on the oxide surface with two Fe atoms located at approximately 3.34 Å. In contrast, XAS studies on Pb(II) sorption onto ferrihydrite, at pH 4.5, reveal two distinct Pb−Fe bond average radial distances of 3.34 and 3.89 Å, suggestive of a mixture of monodentate and bidentate sorption complexes present at the oxide surface. Interestingly, at constant pH, the configuration of the sorption complex is independent of the adsorbate concentration. Hence, Pb(II) sorption to a highly disordered adsorbent such as ferrihydrite can be described by one average type of mechanism. Overall, this information will aid scientists and engineers in improving the current models that predict and manage the fate of toxic metals, such as Pb(II), in the aquatic and soil environments.

Introduction

Iron oxides are ubiquitous in soils and aquatic sediments as discrete particles or coatings on other mineral and organic materials. There is sufficient evidence available to demonstrate that the fate of heavy metal contaminants, such as lead and zinc, in soils and aquatic environments is largely controlled by their interactions with these iron oxides (*1*−*7*). Hence, to understand the mobility and bioavailability of these metal contaminants, their sorption reactions must be understood.

Extensive macroscopic studies have been conducted to assess the sorption edges for the interactions of Pb(II) with goethite (*2, 8*−*10*), hematite (*2*), and hydrous ferric oxide (HFO) (*11, 12*). Ainsworth et al. (*13*) studied sorption−desorption edges of Pb(II) sorption onto amorphous iron oxide as a function of residence time. They reported that Pb(II) remained associated with the oxide surface for up to 21 weeks and that the sorption−desorption process was completely reversible. Abdel-Samad and Watson (*14*) complemented Pb−goethite sorption edge investigations with XPS studies to propose mechanistic models describing the changes in the sorption complexes with pH. Other studies have included isotherms to understand the effect of adsorbate concentration on Pb(II) sorption to goethite (*15*−*18*) and amorphous iron oxide (*18, 19*).

Macroscopic experiments are limited to providing information on bulk equilibrium and kinetic processes. However, to determine molecular mechanisms, a spectroscopic approach is needed. X-ray absorption spectroscopy (XAS) has proven to be a powerful tool in environmental research as it selectively probes the local coordination environment of complexation mechanisms under environmentally relevant conditions (*20*−*31*). The application of XAS in the speciation of Pb-contaminated environments is also well-documented (*5, 6, 32*−*34*). In their XAS studies on Pb(II) speciation in contaminated soils, O'Day et al. (*5*) have identified Pb(II) to be significantly associated with iron oxides. The sorption complexes of Pb(II) with various adsorbents including alumina (*22, 26, 27*), clay minerals such as montmorillonite (*35*), and manganese(III,IV) oxyhydroxide (*36, 37*) have been investigated. In their extensive studies, Bargar et al. (*22, 23*) found that Pb(II) formed mononuclear bidentate inner-sphere sorption complexes with hematite and goethite over a wide range of conditions. Lead is also reported to undergo synergistic sorption with high-affinity anions including chloride (*23*), phosphate (*38*), sulfate (*39*), and carbonate (*40*) to form ternary complexes with goethite. In contrast, Pb−EDTA complexes are observed to remain intact when sorbed to goethite (*25*).

A comparison of the macroscopic results shows that amorphous oxides have larger sorption capacities for metal contaminants than crystalline oxides such as goethite (*41*). Although these oxides have similar structures in that they are composed of chains of octahedral units of FeO_6, ferrihydrite has short-range order and a discontinuous layered structure, which explains its high surface area and sorption capacity (*28*). Manceau et al. (*36*) demonstrated through XAS analyses that Pb(II) forms a mononuclear edge-sharing bidentate complex with HFO. Consistently, Scheinost et al. (*30*) found that, at pH 5, this sorption complex was invariant with reaction time (up to 8 weeks), type of ferrihydrite, and presence of competing ions (Cu) and/or fulvic acid. They attributed this continued slow sorption to intraparticle diffusion (*30*). However, there is a need for a systematic set of mechanistic information on the interactions of Pb(II) with ferrihydrite as a function of pH and adsorbate concentration. In this research, traditional macroscopic studies were complemented with XAS analyses to elucidate the mechanisms controlling Pb(II) sorption to ferrihydrite as a function of pH, ionic strength, and adsorbate concentrations.

Materials and Methods

Macroscopic Studies. All the experiments used ACS reagent-grade chemicals, double-deionized water, and acid-washed polypropylene reactors. All experiments were conducted in a nitrogen glovebox to simulate closed system conditions, at room temperature, and under turbulent hydraulic regime ($Re \geq 2.9 \times 10^5$ with respect to the reactor diameter) to minimize the external mass transfer resistance (*42*). Ferrihydrite was prepared using the modified procedure of Schwertmann and Cornell as described by Scheinost et al. (*30*). Accordingly, after precipitation, the ferrihydrite gel was repeatedly centrifuged and washed with deionized water and

* Corresponding author phone: (302)831-0608; fax: (302)831-0605; e-mail: paras@udel.edu.
† University of Delaware.
‡ DuPont Engineering Technology.

10.1021/es0257927 CCC: $25.00
Published on Web 02/05/2003

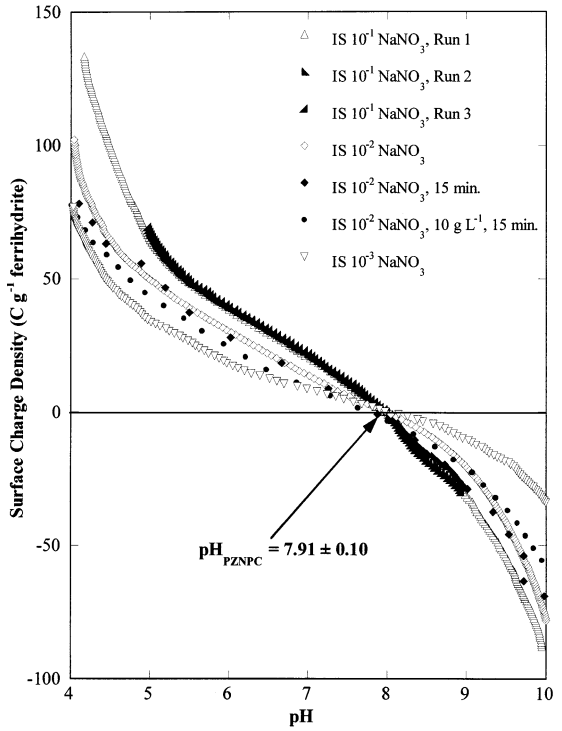

FIGURE 1. Potentiometric titrations of ferrihydrite under closed system conditions at 25 °C. All titrations were conducted using a 2-min contact time and a 1 g L^{-1} suspension, except where noted otherwise.

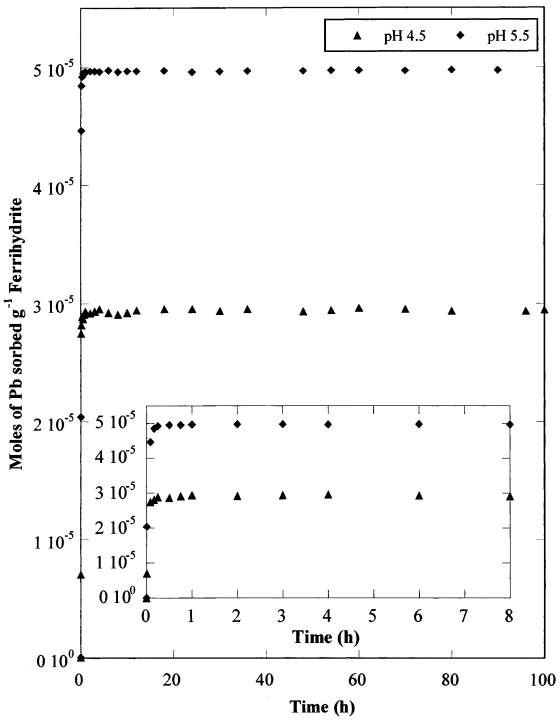

FIGURE 2. Kinetic studies of Pb ($[Pb]_0 = 5 \times 10^{-5}$ M) sorption onto ferrihydrite (1 g L^{-1}) at 25 °C and I.S. 10^{-2} M $NaNO_3$ under closed system conditions and using the chemical boundary conditions employed for traditional isotherms. The inset demonstrates that Pb sorption onto the external surface and along the macropore walls of ferrihydrite particles attains equilibrium in the first few hours of contact time.

aged for 48 h in closed system under turbulent hydraulic conditions. The gel was then used within 2 days for sorption studies. To evaluate the surface charge distribution as a function of pH, potentiometric titrations were performed using 1 g L^{-1} ferrihydrite suspension for three different ionic strengths: 10^{-3}, 10^{-2}, and 10^{-1} M $NaNO_3$ (*41*). The contact time for each titration step was maintained at 2 min. To assess the impact of contact time and suspension solids concentration, additional titration studies were conducted at an ionic strength of 10^{-2} M $NaNO_3$ using a longer contact time of 15 min. At 1 g L^{-1} ferrihydrite, the surface charge distribution did not change significantly with contact time (Figure 1), which is indicative of the rapid kinetics for proton sorption onto ferrihydrite. Similarly, the surface charge distribution obtained using a 10 g L^{-1} ferrihydrite suspension was consistent with the ones obtained using a 1 g L^{-1} suspension. The slight shift to lower surface charge at the higher ferrihydrite suspension concentration is likely due to mass transfer effects. The point of zero net proton charge (pH_{PZNPC}) was determined to be 7.91 ± 0.1 and is consistent with the values reported by others (*41*, *43*, *44*). Interestingly, over the entire pH range employed in this study, the surface charge densities for ferrihydrite are one order smaller than those observed for amorphous HFO but one order greater than those for goethite (*41*). Other physical and chemical characteristics have been described previously (*30*).

Traditional sorption edge and isotherm studies were conducted in 250-mL high-density polyethylene (Nalgene) containers with 1 g L^{-1} oxide to assess the amount of contaminant sorbed to the iron oxide as a function of pH (4.0−8.0), ionic strength (10^{-3}−10^{-1} M $NaNO_3$), and solution concentration [10^{-8}−10^{-3} M $Pb(NO_3)_2$]. The solution concentrations of Pb(II) were maintained below the solubility limits (*45*). To evaluate maximum sorption capacities, additional isotherm studies were conducted with a 0.1 g L^{-1} oxide suspension. Preliminary batch studies were conducted to assess the kinetics of Pb sorption onto the external surfaces of the ferrihydrite particles under different pH conditions. Under the boundary conditions employed for these batch studies, a contact time of 4 h is sufficient for equilibration of Pb sorption onto the external surface as well as onto the macropore walls of the ferrihydrite particles (Figure 2). Consequently, all of the sorption studies presented in this research were conducted with a contact time of 4 h. Samples were collected and filtered using 0.2-μm Gelman Supor-200 filters. The filtrate was acidified and analyzed with graphite furnace atomic absorption spectroscopy (Perkin-Elmer Analyst 800) to determine the bulk aqueous Pb(II) concentrations. For XAS analyses, the suspensions were centrifuged at 12 000*g* for 20 min to ensure maximum solid−liquid separations. The resulting wet pastes were immediately loaded into aluminum or acrylic sample holders, which were sealed with Mylar windows to prevent the loss of moisture.

XAS Data Collection. XAS data were acquired on beamline X-11A at the National Synchrotron Light Source (NSLS), Brookhaven National Laboratory, where the electron beam energy was 2.528−2.8 GeV with a maximum beam current of 280 mA. The XAS data for the Pb−ferrihydrite sorption samples were collected at the Pb L_{III} edge over the energy range of 12.855−13.915 keV in fluorescence mode using a Ge solid-state multi-element detector. For XANES studies, the spectra were collected on the same samples over the energy range of 12.905−13.205 keV at a much higher resolution in fluorescence mode using the same Ge solid-state multi-element detector. The samples were placed 45° to the incident beam. Harmonic rejection was achieved by detuning the monochromator 30% of I_o. The XAS data for the reference compounds were collected over the Pb L_{III} edge in transmission mode. Prior to data collection, the energy was calibrated to the first inflection point of the Pb metal foil (E_o = 13.055 keV). To elucidate the sorption mechanism at room temperature, all the sorption samples as well as reference standards were studied at 298 K.

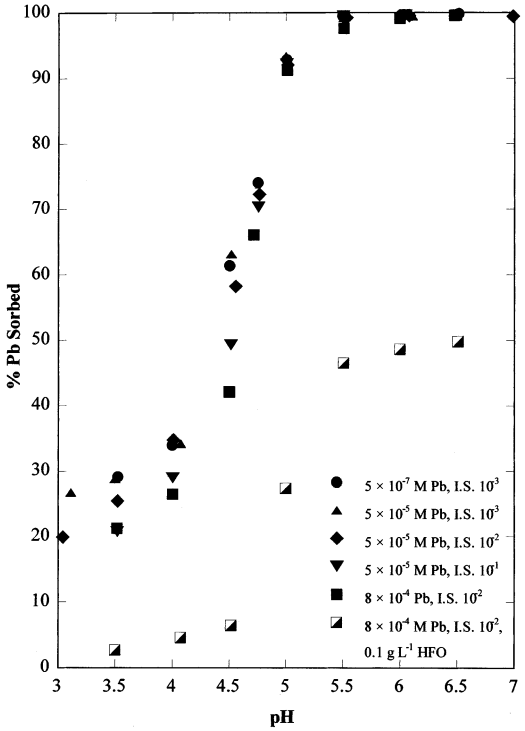

FIGURE 3. pH edges of Pb(II) sorption to ferrihydrite (1 g L^{-1}) under closed system conditions: effect of ionic strength and initial Pb(II) concentrations.

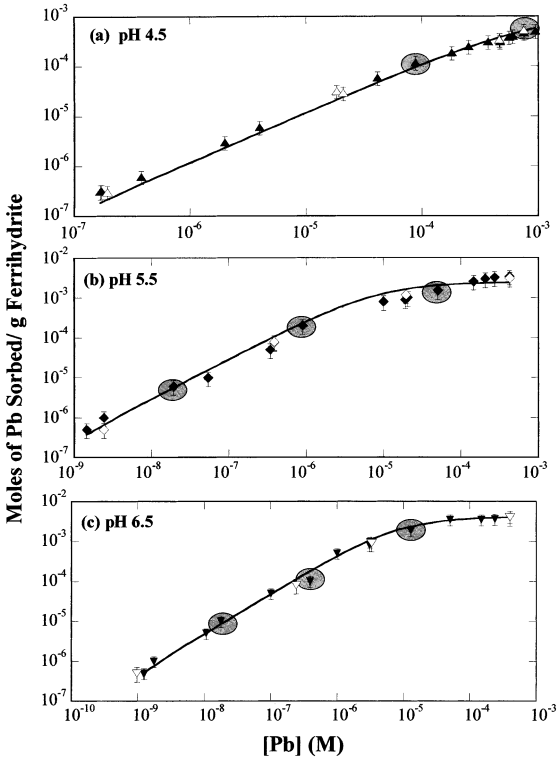

FIGURE 4. Isotherms of Pb(II) sorption to ferrihydrite (1 g L^{-1}) under closed system conditions at 25 °C and I.S. 10^{-2} M $NaNO_3$. Solid symbols represent the isotherm data, and open symbols represent the sorption edge data presented in Figure 3. XAS studies were conducted on data points marked with ovals.

The XAS spectra were analyzed using WinXAS (Version 2.1). For each scan, the background X-ray absorbance was subtracted by fitting a linear polynomial through the pre-edge region. The edge jump of a background-corrected spectrum was normalized with a linear polynomial over 13.155−13.455 keV. The threshold energy (E_o) was determined from the first inflection point in the edge region and was used to convert the spectra from energy to k space. A cubic spline function was employed to account for the atomic absorption in the absence of backscattering contributions over the range 1.95−10.5 $Å^{-1}$. This isolated function produced the XAFS function [$\chi(k)$], which was then weighted by k^3 to enhance the higher k space data. The Bessel window function was used in Fourier transforms to produce the radial structural function (RSF) over 2.4−9.7 $Å^{-1}$ for all sorption samples. These RSF are uncorrected for phase shifts.

To obtain the structural information, the Fourier transforms were fit with an Fe-substituted PbO model generated using FEFF7 (*30*), where all the parameters except the amplitude reduction factor (S_o^2) were allowed to float. A comparison of the $Pb(NO_3)_2$ solution spectra collected in transmission mode with that of the fluorescence mode revealed an average S_o^2 of 0.60, which was used in fitting. In each sample, the E_o shift was constrained to be equivalent for all shells. The value of E_o was constrained to be equal for all the shells in each sample. The number of parameters varied during the fitting was always less than the maximum allowed based on $N_{free} = (2 \times \Delta k \times \Delta R)/\pi$, where N_{free} is the number of degrees of freedom, Δk is the range of k space being fit, and ΔR is the range of the R space (*46*). For any given shell, a good fit was determined on the basis of minimum residual error. Additionally for each sample, the fitting routine was carried out on their individual scans as well as their averaged scan such that the error in the accuracy of the structural parameters for a given shell did not exceed 15%.

Results and Discussion

Sorption Edges. The sorption edges (Figure 3) are sharp sigmoid profiles characteristic of transition metals with pH_{50} ≈ 4.5, which is consistent with the range observed for most other iron oxide studies reported (*8*, *9*, *11*, *13*, *15*, *17*, *19*). Even at low pH values, there was a small amount of Pb(II) sorbed to the oxide surface. In the pH range studied, Pb(II) sorption to ferrihydrite does not significantly vary with ionic strengths between 10^{-3} and 10^{-1} M $NaNO_3$, suggesting that this background electrolyte does not provide significant competition to Pb(II) sorption. Swallow et al. (*47*) also reported Pb(II) sorption to HFO to be unaffected by ionic strengths ranging from 5×10^{-3} to 5×10^{-1} M $NaClO_4$. These results suggest that Pb(II) primarily sorbs to ferrihydrite and goethite to form inner-sphere complexes. In contrast, in clay minerals such as montmorillonite, the Pb(II) sorption mechanism varies from predominantly outer-sphere complexation at lower pH values to a mixture of outer- and inner-sphere complexation at pH > 6.0 (*35*). Lead sorption to montmorillonite is also a function of ionic strength (*35*). In Figure 3, Pb(II) sorption decreased with increasing Pb(II)/ferrihydrite ratio, indicative of the saturation of available sites on the surface of ferrihydrite (*9*). Benjamin and Leckie (*19*) observed a similar shift in the sorption edges for Pb(II) sorption to amorphous $Fe_2O_3 \cdot H_2O$.

Sorption Isotherms. To assess the effect of adsorbate concentrations on Pb(II) sorption to ferrihydrite, traditional isotherm studies were conducted at pH 4.5, 5.5, and 6.5 under closed system conditions at room temperature. For all Pb(II) concentrations, the isotherms are consistent with the sorption edges (Figure 4). Interestingly, in all isotherms at lower Pb(II) concentrations, the amount of Pb(II) sorbed to ferrihydrite is linearly proportional to the dissolved concentration. With increases in Pb(II) concentration, each isotherm forms a plateau indicative of the onset of saturation of sites, which is defined as the maximum sorption capacity available on the ferrihydrite surface (*42*, *48*). This maximum sorption capacity increases with pH (Figure 4). The linear relation between the sorbed Pb(II) concentration and the bulk

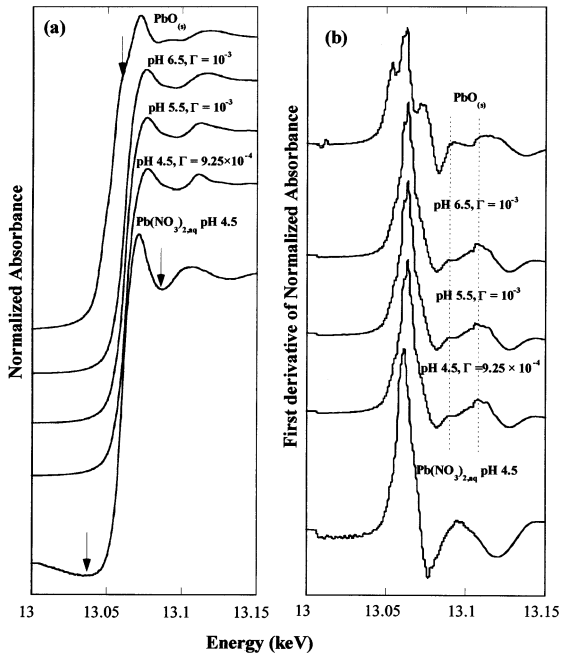

FIGURE 5. Normalized XANES spectra (a) and corresponding first derivatives (b) of Pb−ferrihydrite sorption complexes compared with the Pb references. E_0 for L_{III} edge is at 13.055 keV. The notation Γ in the legends implies adsorption density in mol of Pb sorbed (g of ferrihydrite)$^{-1}$.

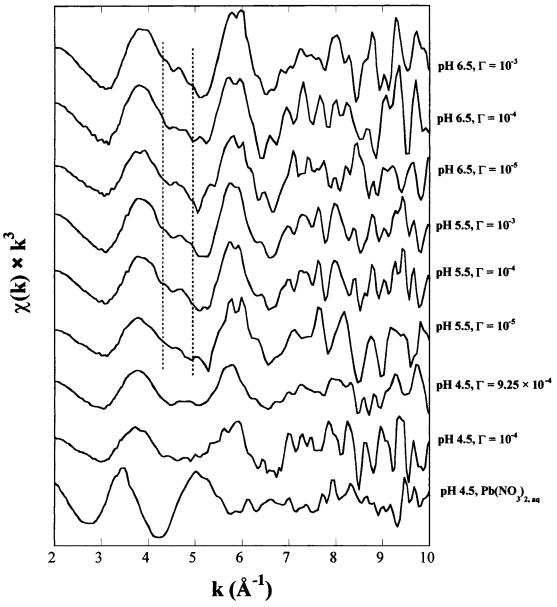

FIGURE 6. Background-subtracted, normalized, and averaged k^3-weighted XAS spectra of Pb−ferrihydrite sorption complexes studied at the Pb L_{III} edge in fluorescence mode as a function of pH and adsorbate loading compared with that of aqueous $Pb(NO_3)_2$ collected in transmission mode. The samples were prepared under closed system conditions and I.S. 10^{-2} M $NaNO_3$. The notation Γ in the legends implies adsorption density in mol of Pb sorbed (g of ferrihydrite)$^{-1}$.

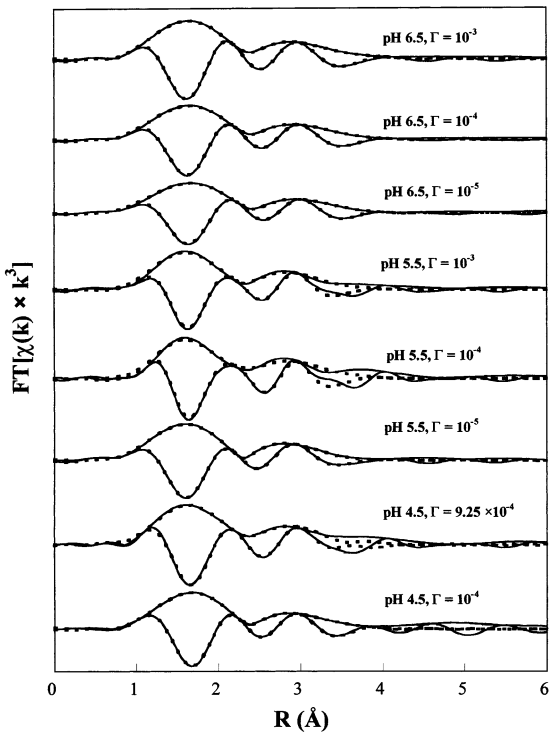

FIGURE 7. Fourier transforms (magnitude + real part) of Pb L_{III} edge XAS spectra of Pb−ferrihydrite sorption complexes (solid lines), presented as a function of pH and adsorbate loading, each filtered with a Fe-substituted PbO model (dashed lines) from 0.6 to 3.85 Å. The notation Γ in the legends implies adsorption density in mol of Pb sorbed (g of ferrihydrite)$^{-1}$.

aqueous Pb(II) concentration at equilibrium (Figure 4) suggests that Pb(II) sorption to ferrihydrite can be described by one average type of site (*42*). This hypothesis will be verified with spectroscopic studies presented in the following sections. The ability of the triple-layer surface complexation model to simulate the experimental data is detailed in an accompanying paper (*49*).

XANES Studies. The sensitivity of Pb L_{III} XANES with respect to the first-shell coordination has been well-documented previously (*22*−*27*, *35*). A comparison of the normalized XANES spectra for the sorption samples and their first derivatives with those of selected Pb references in Figure 5 demonstrates the change in local coordination in the first shell around the Pb atom. The XANES spectrum of aqueous Pb(II) ions shows two distinctive features (Figure 5a): a subtle depression in the pre-edge region between 13.03 and 13.04 keV and a sharp depression above the edge around 13.085 keV. These features are absent in the XANES spectra of the sorption samples, indicating that the Pb(II) ions sorbed onto ferrihydrite have different first-shell coordination than that of aqueous Pb(II) ions. These differences are prominent in the first derivatives of the XANES spectra (Figure 5b) for the aqueous Pb(II) ion and the Pb(II) sorption samples; these differences confirm that the Pb(II) ions do not retain their primary hydration shell upon sorption to ferrihydrite. Interestingly, the XANES features of Pb−ferrihydrite sorption complexes did not vary between pH 4.5 and pH 6.5, suggesting that the first-shell coordinations surrounding the Pb atoms are similar (*23*, *35*). The XANES spectra of the sorption samples in this study resemble those of Pb−goethite and Pb−hematite systems (*23*), suggesting that the sorbed Pb(II) ions have similar coordination environments for all three iron oxides. Furthermore, these XANES spectra are similar to that of $Pb_4(OH)_4^{4+}$(aq) (*26*), thus implying that the first shell of sorbed Pb(II) ions is a distorted trigonal pyramidal coordination with hydroxide ligands or surface oxygen ligands. In contrast, the XANES spectrum of PbO (Figure 5a) and its first derivative (Figure 5b) show a distinct shoulder around 13.045−13.05 keV and two dominant peaks at 13.09 and 13.108 keV. These features are consistent with the ones reported by Chisholm-Brause et al. (*27*) for different polymorphs of PbO and other oxidized complexes of Pb. The pre-edge shoulder in the PbO XANES spectra has been assigned to 2p → 6s electronic transitions that possibly arise

TABLE 1. Structural Parameters of Pb(II)−Ferrihydrite Sorption Complexes[a]

pH	Γ (mol of Pb g^{-1})	atom	CN	R (Å)	σ^2 ($Å^2$)	C_3 ($Å^3$)	C_4 ($Å^4$)	ΔE_0 (eV)	% res.
6.5	10^{-3}	O	2.102 (0.09)	2.274 (0.012)	0.0106	−	−	+5.21	2.70
		Fe	2.379 (0.15)	3.316 (0.028)	0.0127	−	−		
6.5	10^{-4}	O	2.051 (0.10)	2.271 (0.011)	0.0110	−	−	+4.98	3.31
		Fe	2.089 (0.18)	3.334 (0.032)	0.0139	−	−		
6.5	10^{-5}	O	1.973 (0.11)	2.303 (0.014)	0.0117	−	−	+4.82	1.36
		Fe	2.216 (0.17)	3.335 (0.036)	0.0142	−0.0004	−		
5.5	10^{-3}	O	2.014 (0.11)	2.292 (0.012)	0.0097	−	−	+4.41	1.89
		Fe	2.217 (0.17)	3.347 (0.022)	0.0139	−0.0007	−		
5.5	10^{-4}	O	2.210 (0.10)	2.284 (0.012)	0.0118	−	−	+6.14	2.51
		Fe	2.012 (0.11)	3.339 (0.026)	0.0150	−0.0004	−		
5.5	10^{-5}	O	2.106 (0.13)	2.277 (0.014)	0.0131	−	−	+5.56	3.54
		Fe	2.178 (0.14)	3.337 (0.032)	0.0150	−0.0006	−		
4.5	9.25×10^{-3}	O	1.979 (0.12)	2.274 (0.011)	0.0106	0.0003	−	+4.65	7.14
		Fe	1.855 (0.16)	3.334 (0.028)	0.0141	0.0004	−		
		Fe	0.796 (0.20)	3.889 (0.036)	0.0148	−0.0007	0.00001		
4.5	10^{-4}	O	2.477 (0.14)	2.284 (0.014)	0.0111	0.0003	−	+4.31	8.36
		Fe	2.279 (0.22)	3.358 (0.034)	0.0147	0.0002	−		
		Fe	0.656 (0.24)	3.898 (0.033)	0.0151	−0.0006	0.00003		

[a] Fits obtained using Fe-substituted PbO model (*30*). Γ, sorption density (mol of Pb (g of ferrihydrite)$^{-1}$); CN, coordination number; R, average radial distance; σ^2, Debye−Waller factor; C_3, third cumulant; C_4, fourth cumulant. Least-squares precisions are given in parentheses. Typically the uncertainties in N are estimated to be 20% for the first shell and 30% for the second shell. Similarly, variations in R are estimated to be 0.03 Å for all shells.

from multiple scattering of the photoelectron from the neighboring atoms (*22*, *27*). This feature is weak to absent in the Pb−ferrihydrite sorption spectra, which can be attributed to the change in the 2p → 6s transition, which arises from the differences in the Pb−O bond lengths or O−Pb−O angles. Furthermore, the strict exclusion of carbonates in this research eliminates the possibility of the formation of carbonate species. Thus, the sorption complexes have slightly different structures than the ones of commonly occurring lead precipitates.

XAS Studies. The XAS spectra of Pb(II) sorbed to ferrihydrite under various pH and adsorbate concentrations (Figure 6) do not resemble that of Pb^{2+} in aqueous solution, thus confirming that the local coordination of sorbed Pb^{2+} is different than that of the aqueous Pb^{2+} ion. The XAS spectra of the sorption samples are a result of two backscattering envelopes, indicative of two distinct shells surrounding the sorbed Pb(II) ion. All the spectra are noisier in the higher k region, which may be attributed to the presence of highly disordered ferrihydrite present in the background. For each pH, the χ spectra are similar at all sorbate loadings; however, their signal-to-noise ratios improved with sorbate concentration. For systems studied at pH 5.5 and pH 6.5, the XAS spectra show a distinct shoulder present in the χ region of 4−5 $Å^{-1}$, which is absent in the spectra of pH 4.5 sorption systems. This distinction suggests that the mechanism by which Pb(II) sorbs to ferrihydrite is a function of pH. Interestingly, all of these sorption spectra do not resemble those of PbO or $PbCO_3$ (*33*), thus ruling out the possibility of the formation of surface precipitates.

To reveal the local structure of Pb(II) sorbed to ferrihydrite, the χ spectra of sorption samples were Fourier transformed over the range 2.4−9.7 $Å^{-1}$ and then fitted with a theoretical model of Fe-substituted PbO over the range of 0.6−3.8 Å (Figure 7). The structural parameters derived from fitting the Fourier transforms (uncorrected for phase shift) of these spectra confirm the presence of two different neighboring atoms: O in the first shell and Fe in the second shell (Table 1). No meaningful fits were obtained when Pb was considered as a possible contributor to the second shell with or without Fe contributions. Thus, the probability of the formation of surface precipitates is minimal to insignificant (*23*). Furthermore, the absence of Pb backscatterers implies that Pb(II) ions are sorbed to ferrihydrite predominantly as mononuclear sorption complexes.

In all the samples, the first shell is composed of two oxygen atoms at an average radial distance of 2.27−2.29 Å. Resultant structural parameters (Table 1 and Figure 7) for all sorption samples reveal oxygen neighbors in the first shell of the sorbed Pb(II) ion at an average radial distance of 2.28 Å. These radial distances are consistent with other Pb(II) sorption studies (*22*−*24*, *30*, *35*, *36*, *39*). The first shell of fully hydrated Pb(II) ions is reported to be octahedral with the radial distances for Pb−O ranging from 2.47 to 2.49 Å (*22*, *23*, *35*). These radial distances are much larger than the ones observed in the present sorption systems, suggesting that Pb(II) ions did not retain their primary hydration sphere upon sorption to ferrihydrite. Similarly, Pb−O bond distances of 2.69 Å reported for $PbCO_3$ (*33*), 2.32 Å for $Pb_4(OH)_4^{4+}$(aq) (*22*), and 2.32−2.36 Å for lead oxides (*22*, *32*, *33*) are much larger than

the ones reported for the sorption samples, suggesting the absence of surface precipitation reactions.

For sorption systems studied at pH 6.5, the second shell was best fitted with two Fe atoms at an average radial distance of 3.34 Å. The local structure of Pb(II) ion sorbed to ferrihydrite did not change with adsorbate concentration; however, with decrease in adsorbate concentration, the degree of disorder increased as indicated by the Debye−Waller factor (σ^2). Present research also demonstrates that the local structure of the Pb−ferrihydrite sorption complex at pH 5.5 is similar to the one observed at pH 6.5 and is independent of adsorbate concentration. In most samples, the highly disordered ferrihydrite, in the background, hinders obtaining a reasonable and meaningful Gaussian fit for these systems. Consequently, inclusion of a third-order cumulant (C_3) and a fourth order cumulant (C_4) was necessary to account for the disorder arising from skewing of the moments of distribution as well as to measure the weight in the tails of distributions (*50*). Scheinost et al. (*30*) determined similar structural parameters for Pb−ferrihydrite complexes at pH 5.0; they found that the sorption mechanism was independent of the method of oxide preparation, the presence of another metal cation such as Cu, and the reaction contact time. They attributed the increase in Pb(II) sorption with time to intraparticle diffusion (*30*). Collectively, the spectroscopic results corroborate the macroscopic modeling results, implying that the reaction mechanism by which Pb(II) sorbs to ferrihydrite does not change between pH 5.0 and pH 6.5.

Conversely, the sorption samples studied at pH 4.5 reveal two distinct Pb−Fe bond distances of 3.34 and 3.89 Å where the Fe contributions at 3.89 Å bond distance are much smaller than those at 3.34 Å. Bargar et al. (*22*, *23*) found that the Pb−Fe separations in the range of 2.91−3.49 Å arise from edge-sharing bidentate sorption of Pb(II) ions to FeO_6 octahedra, while those separations equal to or greater than 3.90 Å arise from monodentate or corner-sharing bridging-bidentate bonding of Pb(II) ions to FeO_6 octahedra. Thus, with ferrihydrite at pH ≥5.0, Pb(II) ions form mononuclear bidentate edge-sharing complexes (Figure 8a). This result is consistent with others including Pb(II) sorption to goethite and hematite at pH ≥6.0 (*22*, *23*), Pb(II) sorption to alumina at pH ≥6.0 (*22*), Pb(II) sorption to HFO at pH 6.5 (*36*), and Pb(II) sorption to goethite at pH 6 (*39*). At lower pH, at least two of the following distinct Pb−ferrihydrite sorption complexes coexist: mononuclear monodentate, mononuclear bidentate corner-sharing, and mononuclear bidentate edge-sharing complexes (Figure 8b). A similar change in the mechanism of Pb(II) sorption to goethite from pH 5.0 to pH 6.0 was observed by Elzinga et al. (*39*). From their spectroscopic investigations, Strawn and Sparks (*35*) reported that Pb(II) sorbed to montmorillonite via outer-sphere complexation at pH <6.3 and via inner-sphere complexes for pH >6.77. Between pH 6.3 and pH 6.77, they observed Pb(II) forming both types of complexes with montmorillonite (*35*). On the other hand, combined results of Fourier transform infrared (FTIR) and XAS demonstrated that, in the presence of organic chelants such as EDTA, Pb(II) sorbs to goethite via an outer-sphere mechanism that is independent of Pb(II)−EDTA concentration, ionic strength, and pH over the range of 4−6. In the presence of a strong background ligand such as carbonate, Pb(II) forms predominantly corner-sharing bidentate and/or tridentate metal-bridge ternary sorption complexes with goethite at pH ≤5; while at higher pH values Pb(II) forms edge-sharing bidentate and/or tridentate metal-bridge ternary sorption complexes with goethite (*51*). In contrast, in the presence of sulfate, Pb(II) forms corner-sharing metal-bridged ternary complexes with goethite at all pH values (*52*). These ternary complex formations explain the increase in Pb(II) sorption onto goethite in the presence of stronger ligands such as carbonate (*51*), sulfate (*52*), and chloride (*24*).

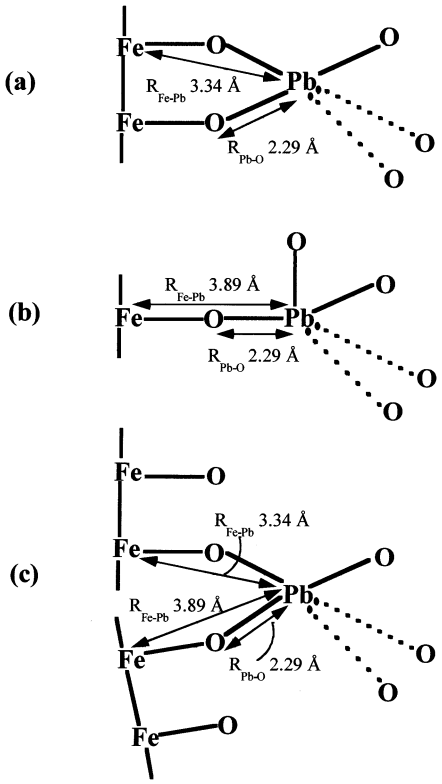

FIGURE 8. Schematic representations of predominant Pb(II)−ferrihydrite sorption complexes based on the interpretations of the XAS analyses at (a) bidentate edge-sharing mononuclear; (b) monodentate mononuclear; and (c) bidentate corner-sharing mononuclear. At pH ≥ 5.0, only configuration a is observed. At pH < 5.0, either a combination of configurations a and b or a combination of configurations b and c is expected.

Interestingly, in all the Pb−ferrihydrite sorption samples, no meaningful fits were obtained when Pb−Pb contributions were included in the fits of the second shell. A lack of these contributions in the sorption samples confirms the absence of the formation of Pb precipitates on the ferrihydrite surface. Overall, the macroscopic and spectroscopic studies presented here demonstrate that Pb(II) ions predominantly sorb to ferrihydrite via inner-sphere complexation, not retaining their primary hydration shell upon sorption. Interestingly, this sorption mechanism transitions from a mixture of monodentate and bidentate sorption complexes at lower pH to predominantly edge-sharing bidentate complexes at higher pH values. Furthermore, this paper demonstrates that, at constant pH, the configuration of the sorption complex is invariant of the adsorbate concentration. Such information will aid scientists and engineers in improving the current models that predict and manage the fate of toxic metals, such as Pb(II), in the aquatic and soil environments. In an accompanying manuscript (*49*), the extensive collection of new macroscopic and spectroscopic data presented in this paper was used to assess the ability of the modified triple-layer model to predict single-solute Pb(II) sorption onto ferrihydrite as a function of pH, ionic strength, and Pb concentration.

Acknowledgments

Funding from the DuPont Company and the State of Delaware through the Delaware Research Partnership supported this research. The authors gratefully thank the technical support of staff at beamline X11A, National Synchrotron Light Source, Brookhaven National Laboratory

(NY). The authors also thank Dr. Noel Scrivner of DuPont Engineering Technology for his valuable input on this research.

Literature Cited

(1) Lion, L. W.; Altmann, R. S.; Leckie, J. O. *Environ. Sci. Technol.* **1982**, *16*, 660−666.
(2) Rose, A. W.; Bianchi-Mosquera, G. C. *Econ. Geol.* **1993**, *88*, 1226−1236.
(3) Lena Q, M.; Gade, N. *J. Environ. Qual.* **1997**, *26*, 788−794.
(4) Martinez, C. E.; McBride, M. B. *Environ. Sci. Technol.* **1999**, *33*, 745−750.
(5) O'Day, P. A.; Carroll, S. A.; Waychunas, G. A. *Environ. Sci. Technol.* **1998**, *32*, 943−955.
(6) Ostergren, J. D.; Brown, G. E., Jr.; Parks, G. A.; Tingle, T. N. *Proc. Natl. Acad. Sci. U.S.A.* **1999**, *96*, 3388−3395.
(7) Dong, D.; Nelson, Y. M.; Lion, L. W.; Shuler, M. L.; Ghiorse, W. C. *Water Res.* **2000**, *34*, 427−436.
(8) Balistrieri, L. S.; Murray, J. W. *Geochim. Cosmochim. Acta* **1982**, *46*, 1253−1265.
(9) Hayes, K. F.; Leckie, J. O. Mechanism of Lead Ion Sorption at the Goethite−Water Interface. In *Geochemical Processes at Mineral Surfaces*; Davis, J. A., Hayes, K. F., Eds.; ACS Symposium Series 323; American Chemical Society: Washington, DC, 1986; pp 114−141.
(10) Lützenkirchen, J. *J. Colloid Interface Sci.* **1997**, *195*, 149−155.
(11) Gadde, R. R.; Laitinen, H. A. *Anal. Chem.* **1974**, *46*, 2022−2026.
(12) Kinniburgh, D. G.; Jackson, M. L.; Syers, J. K. *Soil Sci. Soc. Am. J.* **1976**, *40*, 796−800.
(13) Ainsworth, C. C.; Pilon, J. L.; Gassman, P. L.; VanDerSluys, W. G. *Soil Sci. Soc. Am. J.* **1994**, *58*, 1615−1623.
(14) Abdel-Samad, H.; Watson, P. R. *Appl. Surface Sci.* **1998**, *136*, 46−54.
(15) McKenzie, R. M. *Aust. J. Soil Res.* **1980**, *18*, 61−73.
(16) Rodda, D. P.; Johnson, B. B.; Wells, J. D. *J. Colloid Interface Sci.* **1996**, *184*, 365−377.
(17) Christophi, C. A.; Axe, L. *J. Environ. Eng.* **2000**, *1*, 66−74.
(18) Nelson, Y. M.; Lion, L. W.; Shuler, M. L.; Ghiorse, W. C. *Environ. Sci. Technol.* **2002**, *36*, 421−425.
(19) Benjamin, M.; Leckie. J. *J. Colloid Interface Sci.* **1981**, *79*, 209−221.
(20) Manceau, A.; Charlet, L. *J. Colloid Interface Sci.* **1992**, *148*, 425−442.
(21) Manceau, A.; Charlet, L. *J. Colloid Interface Sci.* **1992**, *148*, 443−458.
(22) Bargar, J. R.; Brown, G. E., Jr.; Parks, G. A. *Geochim. Cosmochim. Acta* **1997**, *61*, 2617−2638.
(23) Bargar, J. R.; Brown, G. E., Jr.; Parks, G. A. *Geochim. Cosmochim. Acta* **1997**, *61*, 2639−2652.
(24) Bargar, J. R.; Brown, G. E., Jr.; Parks, G. A. *Geochim. Cosmochim. Acta* **1998**, *62*, 193−207.
(25) Bargar, J. R.; Persson, P.; Brown, G. E., Jr. *Geochim. Cosmochim. Acta* **1999**, *63*, 2957−2969.
(26) Bargar, J. R.; Towle, S. N.; Brown, G. E., Jr.; Parks, G. A. *Geochim. Cosmochim. Acta* **1996**, *61*, 3541−3548.
(27) Chisholm-Brause, C. J.; Hayes, K. F.; Roe, A. L.; Brown, G. E., Jr.; Parks, G. A.; Leckie, J. O. *Geochim. Cosmochim. Acta* **1990**, *54*, 1897−1909.
(28) Spadini, L.; Manceau, A.; Schindler, P. W.; Charlet, L. *J. Colloid Interface Sci.* **1995**, *184*, 73−86.
(29) Axe, L.; Bunker, G. B.; Anderson, P. R.; Tyson, T. A. *J. Colloid Interface Sci.* **1998**, *199*, 44−52.
(30) Scheinost, A. C.; Abend, S.; Pandya, K. I.; Sparks, D. L. *Environ. Sci. Technol.* **2001**, *35*, 1090−1096.
(31) Trivedi, P.; Axe, L.; Tyson, T. A. *J. Colloid Interface Sci.* **2001**, *244*, 230−238.
(32) Hesterberg, D.; Sayers, D. E.; Zhou, W.; Plummer, G. M.; Robarge, W. P *Environ. Sci. Technol.* **1997**, *31*, 2840−2846.
(33) Manceau, A.; Boisset, M.; Hazemann, J.-L.; Mench, M.; Cambier, P.; Prost, R. *Environ. Sci. Technol.* **1996**, *30*, 1540−1552.
(34) Strawn, D. G.; Sparks, D. L. *Soil Sci. Soc. Am. J.* **2000**, *64*, 144−156.
(35) Strawn, D. G.; Sparks, D. L. *J. Colloid Interface Sci.* **1999**, *216*, 257−269.
(36) Manceau, A.; Charlet, M. C.; Didier, B.; Spadini, L. *Appl. Clay Sci.* **1992**, *7*, 201−223.
(37) Matocha, C. J.; Elzinga, E. J.; Sparks, D. L. *Environ. Sci. Technol.* **2001**, *35*, 2967−2972.
(38) Weesner, F. J.; Bleam W. F. *J. Colloid Interface Sci.* **1998**, *205*, 380−389.
(39) Elzinga, E. J.; Peak, D.; Sparks, D. L. *Geochim. Cosmochim. Acta* **2001**, *65*, 2219−2230.
(40) Villalobos, M.; Trotz, M. A.; Leckie, J. O. *Environ. Sci. Technol.* **2001**, *35*, 3849−3856.
(41) Trivedi, P.; Axe, L. *J. Colloid Interface Sci.* **2001**, *244*, 221−229.
(42) Fogler, H. S. *Elements of Chemical Engineering*, 2nd ed.; Prentice Hall: Englewood Cliffs, NJ, 1992.
(43) Schwertmann, U.; Taylor R. M. In *Minerals in Soil Environments*, 2nd ed.; Dinauer, R. C., Dixon, J. B., Weed, S. B., Eds.; SSSA Series 1; Soil Science Society of America: Madison, WI, 1989; pp 379−479.
(44) Anderson, P. R.; Benjamin, M. M. *Environ. Sci. Technol.* **1990**, *24*, 692−698.
(45) Allison, J. D.; Brown, D. S.; Novo-Gradac, K. J. *MINTEQA2/PRODEFA2: A Geochemical Assessment Model for Environmental System*; Center for Exposure Assessment Modeling, U.S. EPA: Washington, DC, 1991.
(46) Teo, B. K. *EXAFS: Basic Principles and Data Analysis*; Springer-Verlag: Berlin, 1986.
(47) Swallow, K. C.; Hume, D. N.; Morel, F. M. M. *Environ. Sci. Technol.* **1980**, *14*, 1326−1331.
(48) Dzombak, D. A.; Morel, F. M. M. *Surface Complexation Modeling: Hydrous Ferric Oxide*; John Wiley & Sons: New York, 1990.
(49) Dyer, J. A.; Trivedi, P.; Scrivner, N.; Sparks, D. L. *Environ. Sci. Technol.* **2003**, *37*, 915−922.
(50) Dalba, G.; Fornasini, P. *Phys. Rev. B* **1993**, *47*, 8502−8504.
(51) Ostergren, J. D.; Trainor, T. P.; Bargar, J. R.; Brown, G. E., Jr.; Parks, G. A. *J. Colloid Interface Sci.* **2000**, *225*, 466−482.
(52) Ostergren, J. D.; Brown, G. E., Jr.; Parks, G. A.; Persson, P. *J. Colloid Interface Sci.* **2000**, *225*, 483−493.

Received for review May 15, 2002. Revised manuscript received December 9, 2002. Accepted December 13, 2002.

ES0257927